RESEARCH ON THE CONNECTION PERFORMANCE OF STEEL-ALUMINUM SELF-PIERCING RIVET BY RIVETING DIE STRUCTURE PARAMETERS

Anheng WANG[1*], Linran ZHU[1], Tao WANG[1], Chuanwen LING[1]

To alleviate the cracking of the bottom aluminum sheet during self-piercing riveting (SPR) in steel-aluminum connections, Simufact-Forming finite element simulation software was used to simulate and experimentally study the connection between 0.65mm steel sheets and 2.5mm aluminum sheets. The critical stress value for sheet cracking was derived using fracture mechanics theory. The effects of chamfering and depth of the lower part of the joint were discussed. The cross-section of the simulated joint was compared with that of the SPR experiment. When the bottom chamfer was 0.26mm and the depth was 0.8mm, the stress value of the lower sheet is minimized, thereby reducing the occurrence of bottom sheet defects and cracking. The simulation results are consistent with the experimental results, providing a reference for the selection of rivet molds in the riveting process of dissimilar materials.

Keywords: Self-piercing riveting; finite element; steel-aluminum connection; rivet die parameters

1. Introduction

Self-piercing riveting (SPR) is an optimal choice for joining aluminum components, and it is a cold-forming process [1]. It connects two sheets (different or similar materials), where the rivet penetrates the top sheet and locks into the lower sheet to form a mechanical joint [2]. Due to its structural advantages, SPR is widely used in industry to join steel and aluminum sheets. Kim et al. [3] proved the feasibility of joining high-tensile strength steel sheets with different strengths to aluminum alloy sheets through self-piercing riveting (SPR) process. In addition to experimental studies, finite element simulation analysis can also provide effective references [4]. However, incompatibility of materials may lead to poor joint performance and sheet defects. Therefore, it is necessary to optimize the joining process and conditions.

The riveting properties of dissimilar materials (such as steel plates and aluminum sheets) have been extensively studied. Xie et al. [5] proposed an

[1] School of Mechanical and Automotive Engineering, Anhui Polytechnic University, Wuhu 241000, China,
*(corresponding author), wahazf@ahpu.edu.cn

integrated optimization methods that covers material, structure, process, and performance in riveting scenarios, aiming to determine the optimal rivet parameters and achieve optimized design of process parameters. The hardness of rivets is crucial. Karathanasopoulos and Mohr [6] found that the joints formed by H4 rivets would not fail during loading through 7 sets of joint failure tests. The improvement of connection technology has received a lot of attention, but rigid tools cannot be adjusted frequently to adapt to boundary conditions, resulting in poor connection quality. Kappe et al. [7] investigated a new connection method V-SPR to adapt to the switching of material thickness and type. Uhe and Meschut [8] used heat treatment and material modification methods to optimize traditional rivets. The developed rivets can be connected using ultra-high-strength steel. Vorderbrüggen et al. [9] found that radial compressive stress was the main cause of failure, and targeted geometric adjustment was made to rivets and molds. Compared SPR with spot welding, Asati et al. [10] found that mold depth was an important parameter for joint cross-section analysis. Liu et al. [11] discovered the influence of mold boundaries on SPR, analyzed the forming process, and concluded that the expansion size of rivets increases with the increase of mold diameter and decreases with the increase of depth. Wituschek and Lechner [12] investigated the combination of roll bending riveting with SPR to obtain better mechanical connections. Karim et al. [13] found that the steel aluminum combination produced the highest joint strength when studying various material combinations for riveted joints.

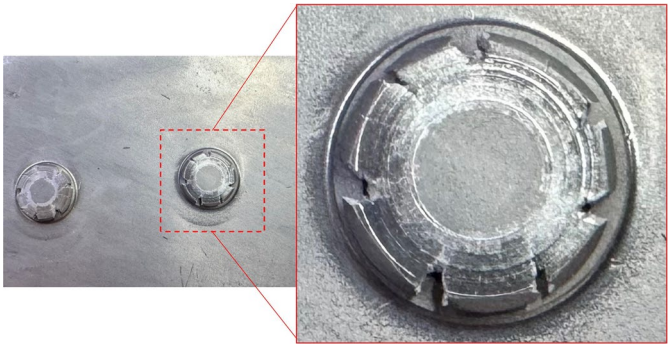

Fig.1 Schematic diagram of bottom sheet cracking

In the past, most of the design optimizations for die geometric parameters have centered on the die. However, during actual production, due to the low ductility of aluminum, the bottom sheet often cracks when using a flat-bottom riveting die for riveting. Fig. 1 shows the cracking at the joint bottom. Cracks often appear on the bottom plate, which are more common in the area where the bottom is formed. We select 0.65-mm-thick steel sheets and 2.5-mm-thick aluminum sheets as the test materials. The geometric parameters of the rivets were

determined, and the chamfering and bottom depth of rivets were designed as variable parameters. Then finite element (FE) software was used to analyze the influence of different parameters on the joint interlocking performance and sheet cracking behaviors. Finally, experimental verification was conducted to validate the FE analysis results.

2. Materials and methods

2.1 Experimental equipment

The SPR requires special equipment, as shown in Fig. 2. The die was fixed; the rivet was placed in the riveting gun, and the sheets to be connected were placed on the punch. After turning on the power, start the device on the controller to prepare the connector.

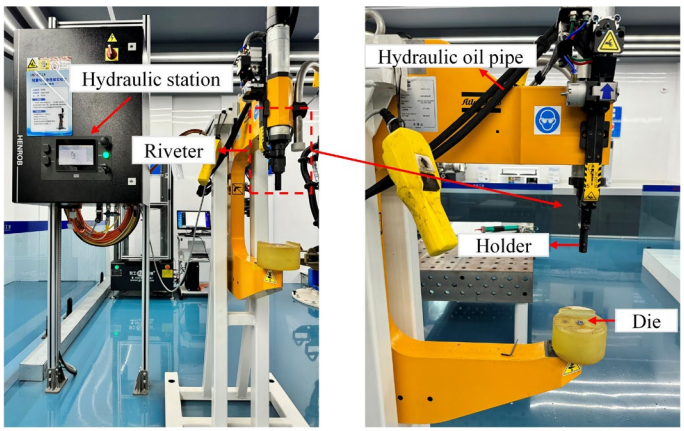

(a) (b)

Fig. 2 SPR test setup, (a) is an overview of the equipment and device and (b) is a side view of the riveter

2.2 Dies

Given that the rivet die designed is a non-standard component, and considering the impacts of manufacturing tolerances and costs, two sets of parameters with the optimal simulation results are selected for physical verification. The dimensions of the riveting die are shown in Fig. 3.

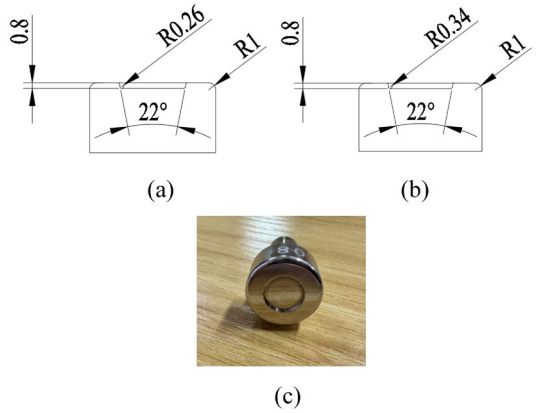

Fig. 3 Geometric parameter model and physical object of riveting die

2.3 Experimental materials

Materials are subjected to shear and tensile stresses during the rivet installation. Cracking is often associated with the insufficient ductility of a material. Table 1 shows specific material properties of the sheet. The stress-strain curve of the aluminum sheet is shown in Fig. 4.

Table 1

Basic properties of materials

Samples	Tensile strength(Rm/MPa)	Yield strength (MPa)	Post-break extension rate(%)	Hardness (HV5)
RGA6 (Al)	261	126	5.7	75.5
DC56D+Z	350	154	34	145

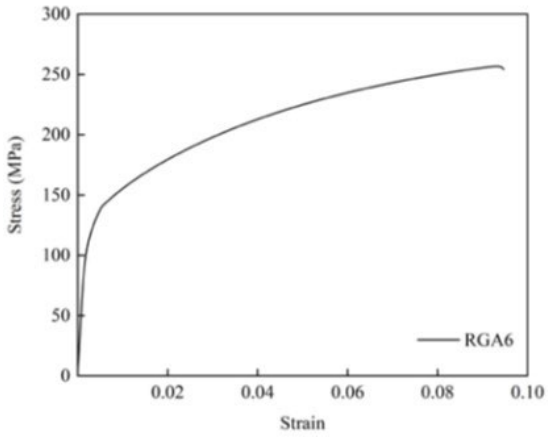

Fig. 4 Stress-strain curve of aluminum sheet

2.4 SPR joints

To investigate the differences in interlocking and mechanical properties between SPR joints, experimental and analytical procedures are implemented: SPR joints were cut using a precision metal cutting machine, and an optical microscope was used to characterize the cross-sectional geometry of the joints. It is worth noting that different boundary conditions will lead to changes in the formation and performance of SPR joints. As shown in Fig. 5, differences in interlocking behavior can be evaluated using three key parameters: width *x*, thickness *h*, and flushness *f*.

Lap shear test is shown in Fig. 6. After the aluminum sheet and steel sheet are overlapped, the tensile testing machine is used for a shear test and obtain the tensile strength of the joint.

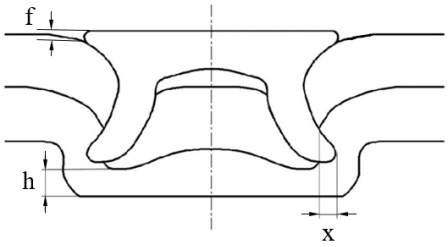

Fig. 5 Geometric characterization of SPR joints

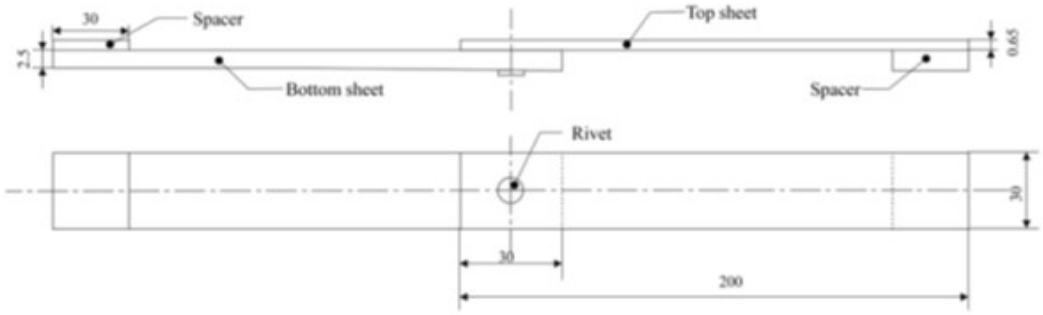

Fig. 6 Size of SPR shear lap test specimen (size unit: mm)

2.5 Theoretical analysis and establishment of critical stress criterion

Floor cracking in SPR is characterized by the emergence and propagation of cracks under stress concentrations. Based on the theory of fracture mechanics, the stress field strength of the crack tip is characterized by the stress intensity factor *K*, which controls the cracking conditions of the crack [14]. For type I (open) cracks, K is expressed as follows:

$$K_I = Y \cdot \sigma \cdot \sqrt{\pi\alpha} \tag{1}$$

where Y is the geometric correction factor; σ is the nominal tensile stress applied on the crack surface (the maximum principal tensile stress in the crack-prone area); and α is the characteristic size of the crack (the depth of the semi-elliptical crack). When $K_I \geq K_{IC}$ (plane stress fracture toughness of the material), the crack becomes unstable and propagates.K_{IC} is expressed as follows:

$$K_{Ic} = \frac{\sigma_{max}}{t \cdot \sqrt{l}} \cdot Y \tag{2}$$

where l is the width of the sheet.

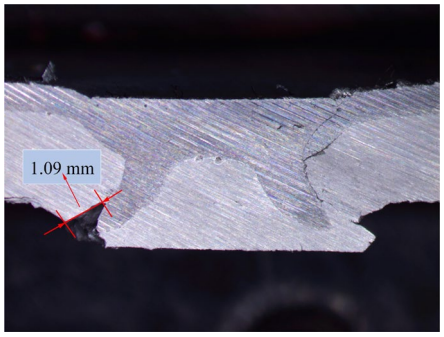

Fig. 7 Crack depth in joint cross-section

For the riveting structure of the 0.65 mm steel sheet and 2.5 mm aluminum sheet, the cracking of the bottom sheet mostly occurs in the geometric discontinuity area at the bottom edge of the riveting die. This region can be considered equivalent to a semi-elliptical surface crack model at the edge. The bottom sheet is subjected to tensile and shear composite stresses during the riveting process. However, its cracking is mainly dominated by normal tensile stress. Therefore, the plane stress assumption is adopted, and the geometric correction factor Y can be determined by the formula for edge semi-elliptical cracks in the fracture mechanics manual [15].

$$Y = 1.12 - 0.23\frac{\alpha}{t} + 10.6\left(\frac{\alpha}{t}\right)^2 - 21.7\left(\frac{\alpha}{t}\right)^3 + 30.4\left(\frac{\alpha}{t}\right)^4 \tag{3}$$

where t is the thickness of the sheet. When $\alpha \ll$t is a shallow crack, the calculation of the critical stress can be simplified to Y≈1.12. The maximum main tensile stress σ is simplified to a maximum stress of 290MPa applied to the riveter. As shown in Fig. 7, the crack depth$\alpha$is 1.09 mm. Therefore, the crack critical stress of the 2.5 mm aluminum sheet is 190.08MPa.

2.6 Simulation model

To enhance simulation efficiency, a self-piercing riveting (SPR) model is established in the finite element simulation software Simufact-Forming using a 2D axisymmetric finite element (FE) approach. As shown in Fig. 8, the model consists of a punch, holder, rivet, rivet die, and sheets. In these components, the rivet and sheets undergo significant plastic deformation during the SPR process. Consequently, the meshing of key deformation zones should be refined, which can help improve calculation efficiency and solve the non-convergence of simulation results. As shown in Fig.8, the mesh element side length of the rivet is set to 0.05 mm with a coarseness level of 2. For the upper sheet, the mesh element side length is configured to 0.14 mm and the refinement level to 1. Similarly, the lower sheet is assigned a mesh element side length of 0.2 mm and a refinement level of 1. The punch, holder, and rivet die in the model are defined as rigid bodies. The friction between components adopts a combined friction model, with a Coulomb friction coefficient of 0.1 and an interface friction coefficient of 0.2. A die spring is integrated into the holder to secure the sheets and suppress sheet warping. Given that the riveting process is dynamic, hydraulic equipment is incorporated into the punch assembly to simulate the self-piercing riveting. The speed of the hydraulic equipment is set to 20 mm/s, and the total stroke of the punch is generally slightly shorter than the rivet length. In this case, it is specified as 4.6 mm.

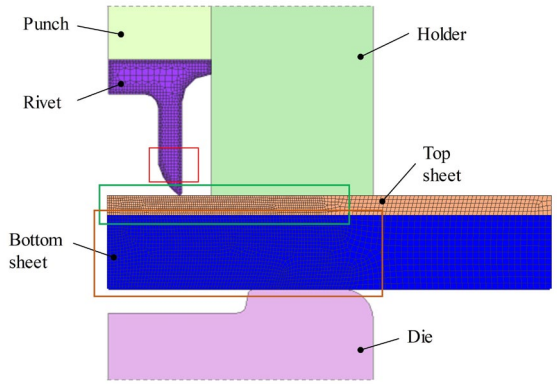

Fig. 8 Schematic diagram of the SPR simulation model

3. Results and analysis

3.1 Experimental results

First, the SPR process is used to connect the 0.65mm steel sheets and the 2.5mm aluminum sheets on the flat-bottomed die with two bottom chamfering

parameters. As shown in Fig.9, the deformation of the test joint is similar to that of the FE connector.

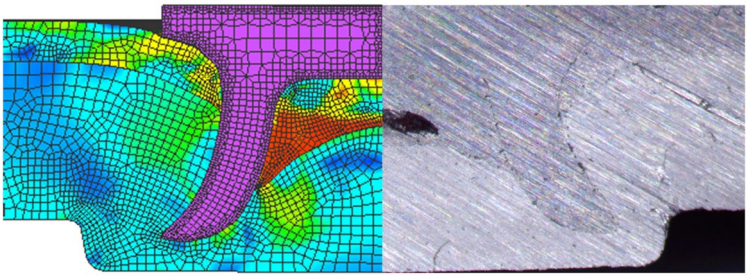

Fig. 9 Comparison of SPR joint cross-section with finite element simulation

Fig. 10 shows the SPR joint and its cross-sectional view. It can be seen that the sheet joint formed using a die with a bottom chamfer of 0.26mm is structurally flat and has the smallest cracks. In addition, in the joint geometric parameters of the two dies, the values of residual thickness (h) and flushness (f) are similar. However, their tensile angles are different. Specifically, the die with a 0.26-mm bottom chamfer has a large opening angle, resulting in an optimal sheet interlocking effect and enhanced joint strength and quality. Fig. 11 shows the shear-tensile test curves, demonstrating that the die with a 0.26-mm bottom chamfer has high tensile load-bearing capacity, ultimately leading to high joint strength.

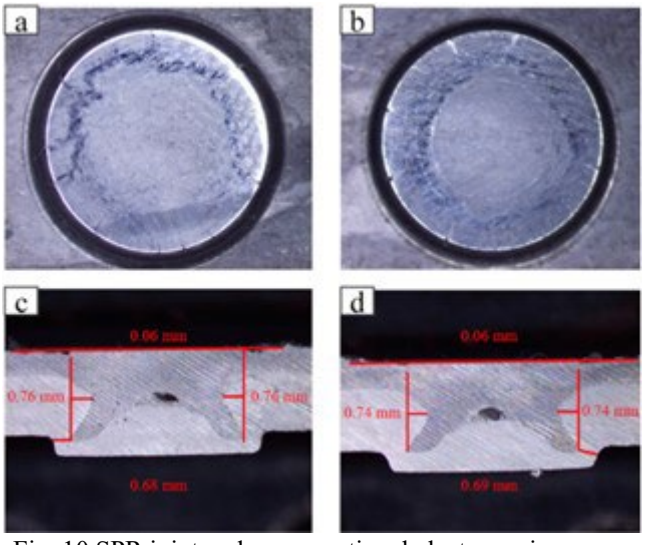

Fig. 10 SPR joint and cross-sectional electron microscopy

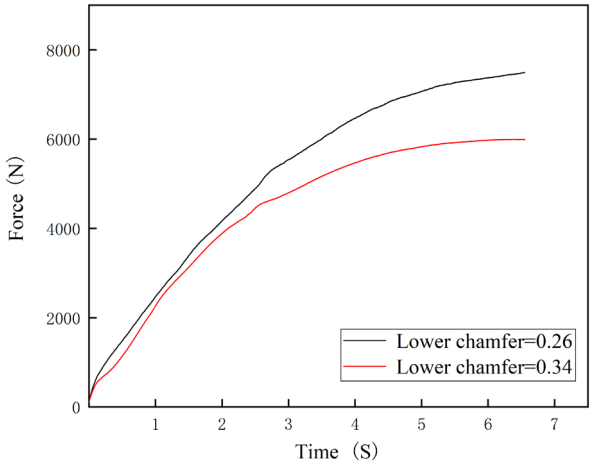

Fig. 11 Shear lap test curve

3.2 Finite element simulation results

When the diameter and depth of the die are fixed, the chamfer at the die bottom is a key parameter of SPR. Proper chamfer parameters alleviate stress concentration and then reduce the probability of sheet defects. Based on the material properties of aluminum sheets and the fracture formula, it can be concluded that abnormal material changes occur when the stress of the lower sheet exceeds 190.08 MPa during the riveting process. Accordingly, the stress value of the cracking zone in the simulation is analyzed. In this study, the rivet die was set with a diameter of 9 mm and a depth of 0.8 mm. To more intuitively observe the forming effect under different chamfers and stress values of the bottom sheet, finite element simulation is employed for calculation and analysis. Fig. 12 shows the simulated stress nephogram of the joint cross-section for different bottom chamfers of the rivet die. The equivalent stress cloud map shows that within the chamfer range of 0.04-0.24mm, the stress value in the cracking zone gradually decreases; within the chamfer range of 0.34-0.54mm, the stress value in the crack prone area gradually increases. In addition, the high stress areas in the crack prone zone also exhibit the same trend of change.

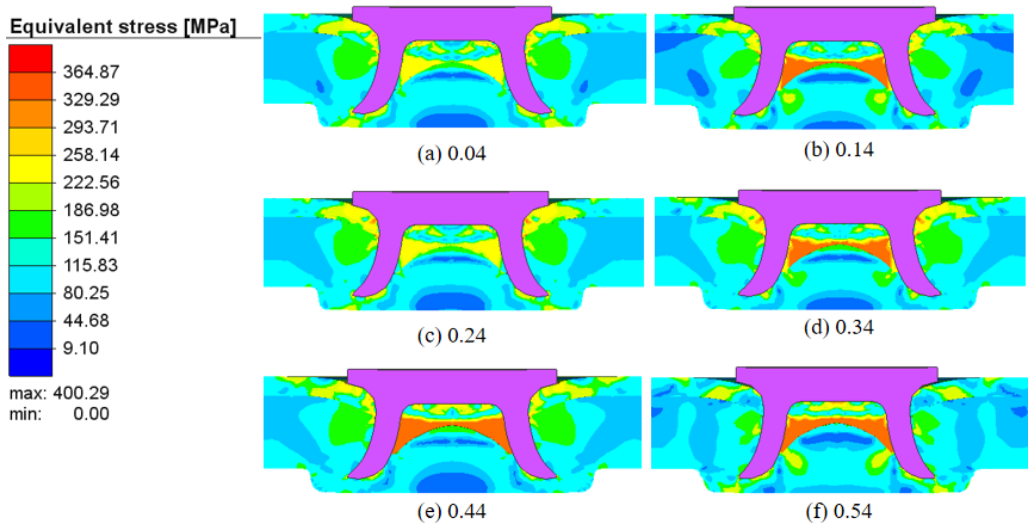

Fig. 12 Simulated stress contours of cross-sectional joints with different bottom chamfers of riveting dies

In the preliminary exploration of the chamfer value, a law is found. As the chamfer value increases in a unit of 0.1mm, the stress value of the bottom sheet increases first and then decreases, and the transition range is 0.24-0.34mm. Therefore, the approximate optimal chamfer will appear within this interval. Further narrowing the range to explore, Fig. 13 shows the simulated stress cloud diagram of the joint with different bottom chamfers of the rivet die, with an average of four chamfer values selected in the range of 0.24-0.34mm. When the cloud map clearly identifies 0.26 mm, the bottom condition and the seam quality are optimal.

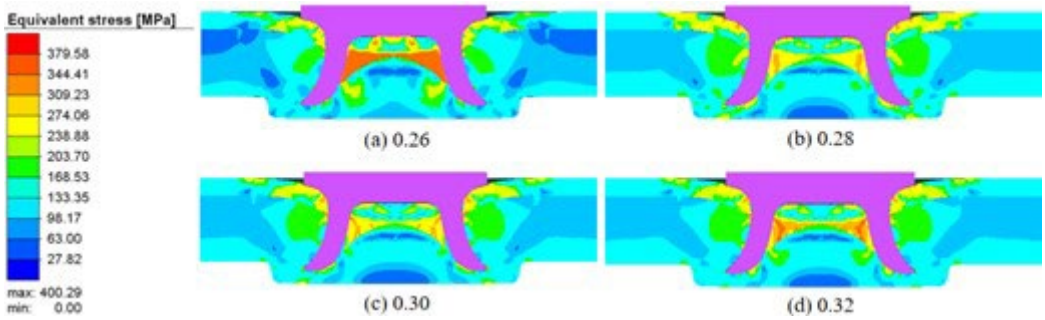

Fig. 13 Simulated stress contours of cross-sectional joints with different bottom chamfers of riveting dies

Fig. 14 shows the yield stress dot line diagram of the lower sheets of SPR, which is convenient for comparison. In the range of 0.04 mm-0.24 mm in Fig. 14(a), due to the expansion of the chamfer, the stress of the lower plate is relieved

to a certain extent in the deformation of the rivet. Therefore, the stress value in this interval decreases gradually. The bigger the chamfer, the better. In the range of 0.34 mm-0.54 mm, when the chamfer reaches a critical point, the rivet squeezes the lower sheet, and the lower plate will contact the mold area earlier, increasing the risk of cracking. It can be found that the stress value of this area gradually increases, as shown in Fig. 14(b). After reaching the critical value, if the chamfer is continued to increase, it will not prevent cracking, but will aggravate the cracking problem.

The trend presented in the line chart is consistent with the trend of the stress cloud map: when the bottom chamfer is 0.26mm, the stress value reaches its minimum value of 168.53MPa. This value is lower than the critical stress of 190.08MPa for aluminum plate cracking. In addition, by combining the trend of stress changes with the theoretical critical value, it can be concluded that a bottom chamfer of 0.26-mm is the optimal parameter because it can effectively solve the problem of bottom plate cracking.

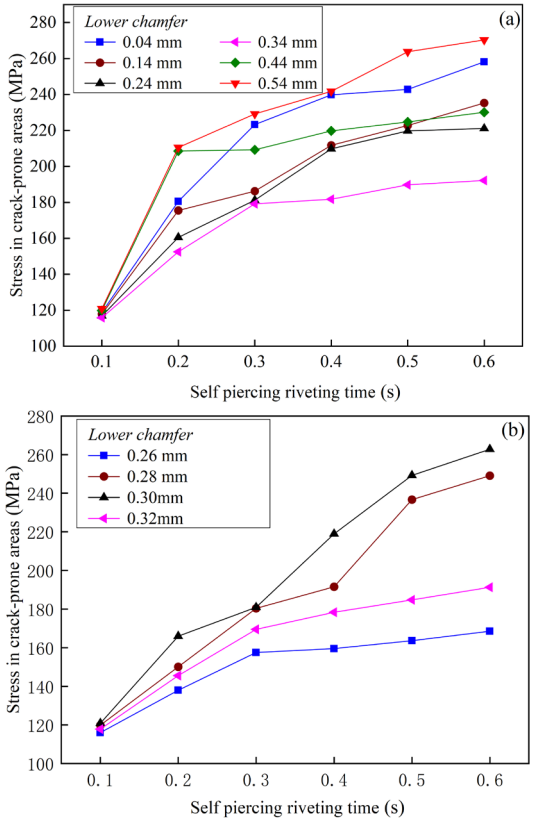

Fig. 14 Point line diagram of the yield stress of the plate during the riveting process

Fig. 15 shows the simulated stress cloud diagram of the joint cross-section under different depths of the riveting die. The results indicate that when the die depth is 0.8 mm, the bottom aluminum sheet has the minimum stress, confirming that this die depth is the optimal parameter for the riveting process.

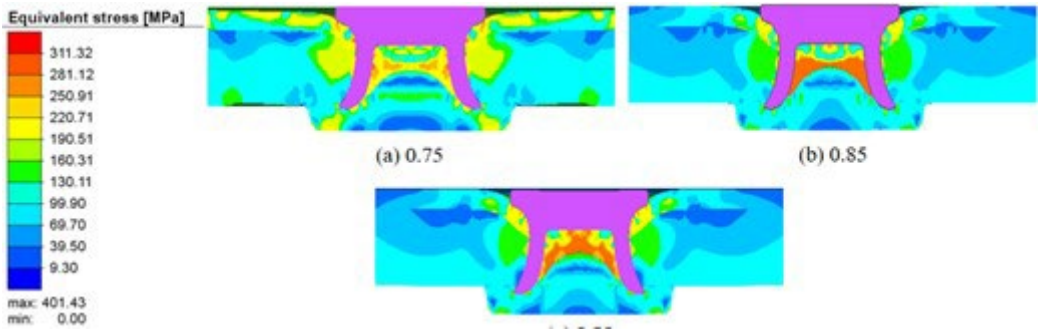

Fig. 15 Simulation stress cloud diagram of joint cross-section at different depths of rivet dies

4. Conclusions

Taking 0.65-mm-thick steel sheets and 2.5-mm-thick aluminum sheets as the research objects, the Simufact-Forming finite element simulation software was used for simulations. Specifically, the critical stress value for aluminum sheet cracking (190.08 MPa) was derived through fracture mechanics theory. In addition, the influence of the bottom chamfer and depth of the flat-bottom rivet die on the forming quality of riveted joints and the stress distribution of the bottom aluminum sheet was analyzed. The following conclusions are drawn:

1) When the diameter of the rivet die was fixed at 9 mm, and the bottom chamfer was 0.26 mm with a depth of 0.8 mm, the stress value of the lower aluminum sheet was the lowest (168.53MPa). This is much lower than the critical stress, which can effectively reduce the defects and cracking of the bottom sheet. Under this parameter, the larger the opening angle of the joint, the better the interlocking effect, and the stronger the joint strength in the shear tensile test;

2) The finite element simulation results are highly consistent with the cross-sectional morphology of the experimental joint, and the stress distribution law is consistent, verifying the reliability of the simulation model. The comparison of different chamfer and depth parameters shows that appropriate riveting die structure parameters can improve the connection performance by reducing the stress concentration.

This study clarifies the optimal parameter combination of chamfer and depth of the bottom of the rivet die in steel-aluminum self-piercing riveting. It provides a theoretical basis and experimental reference for the selection of rivet dies for riveting of dissimilar materials (especially steel and aluminum).

Acknowledgements

This work was funded by the Natural Science Foundation of Anhui Province of China (2208085QE154) and the 2024 Anhui Province University Science and Engineering Teachers' Internship Program in Enterprises (32).

REFERENCES

[1] *Ang, H. Q.,* An overview of self-piercing riveting process with focus on joint failures, corrosion issues and optimisation techniques. Chinese Journal of Mechanical Engineering, vol. 34, no. 1, pp. 2, 2021. https://doi.org/10.1186/s10033-020-00526-3

[2] *Li, D., Chrysanthou, A., Patel, I., & Williams, G.,* Self-piercing riveting-a review. The International Journal of Advanced Manufacturing Technology, vol. 92, pp. 1777-1824, 2017. https://doi.org/10.1007/s00170-017-0156-x

[3] *Kim, M. G., Jeong, T. E., Kam, D. H., & Kim, J.,* Self-piercing rivetability of steel/aluminum and its improvement using reinforcing plate. Journal of Manufacturing Processes, vol. 121, pp. 1-8, 2024. https://doi.org/10.1016/j.jmapro.2024.05.006

[4] *Abe, Y., Kato, T., & Mori, K.,* Joinability of aluminium alloy and mild steel sheets by self piercing rivet. Journal of Materials Processing Technology, vol. 177, no. 1-3, pp. 417-421, 2006. https://doi.org/10.1016/j.jmatprotec.2006.04.029

[5] *Xie, C., Wang, D., Kong, D., Wang, S., & Du, C.,* Material-structure-process-performance integrated optimization method of steel/aluminum self-piercing riveted joint. The International Journal of Advanced Manufacturing Technology, vol. 132, no. 3, pp. 2045-2059, 2024. https://doi.org/10.1007/s00170-024-13483-1

[6] *Karathanasopoulos, N., & Mohr, D.,* Strength and failure of self-piercing riveted aluminum and steel sheet joints: multi-axial experiments and modeling. Journal of Advanced Joining Processes, vol. 5, pp. 100107, 2022. https://doi.org/10.1016/j.jajp.2022.100107

[7] *Kappe, F., Wituschek, S., Bobbert, M., Lechner, M., &Meschut, G.,* Joining of multi-material structures using a versatile self-piercing riveting process. Production Engineering, vol. 17, no. 1, pp. 65-79, 2023. https://doi.org/10.1007/s11740-022-01151-w

[8] *Uhe, B., & Meschut, G.,* Advanced self-piercing riveting of ultra-high-strength steel through rivets with modified material properties. Journal of Manufacturing Processes, vol. 125, pp. 354-363, 2024. https://doi.org/10.1016/j.jmapro.2024.07.037

[9] *Vorderbrüggen, J., Köhler, D., Grüber, B., Troschitz, J., Gude, M., & Meschut, G.,* Development of a rivet geometry for solid self-piercing riveting of thermally loaded CFRP-metal joints in automotive construction. Composite Structures, vol. 291, pp. 115583, 2022. https://doi.org/10.1016/j.compstruct.2022.115583

[10] *Asati, B., Shajan, N., VT, A. K., Arora, K. S., & Narayanan, R. G.,* A comparative investigation on self-piercing riveting and resistance spot welding of automotive grade dissimilar galvanized steel sheets. The International Journal of Advanced Manufacturing Technology, vol. 123, no. 3, pp. 1079-1097, 2022. https://doi.org/10.1007/s00170-022-10226-y

[11] *Liu, Y., Li, H., Zhao, H., & Liu, X.,* Effects of the die parameters on the self-piercing riveting process. The International Journal of Advanced Manufacturing Technology, vol. 105, pp. 3353-3368, 2019. https://doi.org/10.1007/s00170-019-04567-4

[12] *Wituschek, S., & Lechner, M.,* Investigation of the influence of the tumbling angle on a tumbling self-piercing riveting process. Proceedings of the Institution of Mechanical Engineers, Part L: Journal of Materials: Design and Applications, vol. 236, no. 6, pp. 1302-1309, 2022.
[13] *Karim, M. A., Murugan, S. P., Bae, K., Baek, J., Ji, C., Noh, W., Park, Y. D.,* Effect of top sheet materials on joint performance of self-piercing riveting. Journal of Welding and Joining, vol. 40, no. 6, pp. 512-524, 2022. https://doi.org/10.5781/JWJ.2022.40.6.7
[14] *Liu, Z.T., Gao, W., Jin, Y.H., Shangguan, X.F.,* Study on Fracture Toughness of Foundry Aluminum Alloy A356.0(In Chinese).Hot Working Technology, no. 16, pp. 44-46, 2008.
[15] *Gdoutos, E.E.,* Fracture mechanics: an introduction[M]. Dordrecht: Springer Netherlands, 2020.